Origin of tension-compression asymmetry in ultrafine-grained fcc metals

T. Tsuru

Phys. Rev. Materials **1**, 033604 — Published 9 August 2017

DOI: 10.1103/PhysRevMaterials.1.033604

Origin of tension/compression asymmetry in ultrafine-grained fcc metals

T. Tsuru[1,2]

[1]*Nuclear Science and Engineering Center, Japan Atomic Energy Agency, 2-4 Shirakata, Tokai-mura, Ibaraki, Japan*
[2]*Elements Strategy Initiative for Structural Materials (ESISM), Kyoto University, Yoshida, Honmachi, Sakyo-ku, Kyoto 606-8501, Japan*

(Dated: July 21, 2017)

A new mechanism of anomalous tension/compression (T/C) asymmetry in ultrafine-grained (UFG) metals is proposed using large-scale atomistic simulations and dislocation theory. Unlike coarse-grained metals, UFG Al exhibits remarkable T/C asymmetry of the yield stress. The atomistic simulations reveal that the yield event is not related to intragranular dislocations but caused by dislocation nucleation from the grain boundaries (GBs). The dislocation core structure associated with the stacking fault energy in Al is strongly affected by the external stress compared with Cu; specifically, high tensile stress stabilizes the dissociation into partial dislocations. These dislocations are more likely to be nucleated from GBs and form deformation twins from an energetic viewpoint. The new mechanism, which is completely different from well-known mechanisms for nanocrystalline and amorphous metals, is unique to high-strength UFG metals and can explain the difference in T/C asymmetry between UFG Cu and Al.

INTRODUCTION

The plastic deformation of coarse-grained metals is determined by the average collective motion of dislocations because the initial stage of plastic deformation is related to the activation of the pre-existing dislocation sources. The subsequent interaction between dislocations in different slip planes contributes to the hardening process. Grain refinement has generally been used to improve the strength. The interaction between piled-up dislocations and grain boundaries (GBs) plays a dominant role in determining the strengthening of materials according to the well-known Hall–Petch (H–P) relationship [1, 2]. Recent metal processing techniques enable the effective control of the grain size and microstructure in metallic systems. It is possible to produce ultrafine-grained (UFG) metals (100 nm $<$ d $<$ 1 μm; d is the grain size) through severe plastic deformation (SPD) processing [3–6] such as accumulative roll bonding, and these UFG metals exhibit unique and excellent mechanical properties [7–9]. However, the mechanical properties of UFG metals cannot be simply predicted from the average collective motion of intragranular dislocations. The strength of UFG metals is much higher than that predicted using the H–P relation [10, 11]. The strength of nanocrystalline (NC) metals (d $<$ 20 nm) decreases with decreasing grain size, which is generally known as the inverse H–P effect [12, 13]. Although GB sliding and thermally activated local shear have been proposed as underlying deformation mechanisms of NC metals [14–17], they should not be considered the key mechanisms explaining the unique deformation behavior of UFG metals. UFG metals are expected to have a different deformation mechanism than coarse-grained or NC metals because unlike coarse-grained metals, the grain size of UFG metals is too small to accommodate numerous pre-existing dislocations in a grain, and unlike NC metals, the grain size is too large for GB sliding. A different type of dislocation–GB process is thus expected to become dominant. UFG metals have been shown to exhibit anomalous deformation behavior associated with higher stress conditions. For example, the Bauschinger effect has been reported for UFG metals [18–20], in which the microscopic defect texture generated by SPD affects the subsequent plastic deformation.

Tension/compression (T/C) asymmetry is also considered a unique property of UFG metals [18, 21–23]. T/C asymmetry has been widely observed in various metals and alloys. Mg and Mg alloys exhibit definite T/C asymmetry, and the mechanism for this behavior is known to be asymmetric twinning deformation of the hexagonal-close-packed (hcp) structure [24–26]. T/C asymmetry of amorphous metals was observed to be caused by the atomic-pair distribution with nucleation of shear bands [27], and that observed in NC metals was explained by the same mechanism [28]. The deformation mechanism and T/C asymmetry in NC metals were preliminarily examined for direct comparison [29]. However, the T/C asymmetry of UFG metals cannot be understood by any previously proposed mechanism. UFG Al exhibited definite T/C asymmetry, where the strength under compression was higher than that under tensile loading ($\tau_T < \tau_C$) [21], whereas UFG Cu did not exhibit clear asymmetry [18]. Therefore, an unknown mechanism that is associated with the difference between UFG Cu and Al underlies the T/C asymmetry of UFG metals.

A number of atomic-scale simulations have been implemented to investigate the deformation behavior of NC metals [30–34], and the amorphous-like T/C asymmetry in these materials was confirmed [33, 34]. However, it remains difficult to capture the anomalous deformation behavior of UFG metals because unlike NC metals [29], both inter- and intragranular dislocation contribute dominantly to plastic deformation. In this study, I developed parallelized molecular dynamics and visualization codes to simulate three-dimensional polycrystalline models including intergranular dislocation sources and explored a new mechanism of T/C asymmetry for UFG metals.

ANALYSIS METHOD

Atomic models of polycrystalline face-centered-cubic (fcc) Cu and Al were constructed using the Voronoi polyhedral division technique. Intragranular dislocation should be considered to capture the deformation behavior of UFG metals as previously mentioned. In this study, Frank-Read (FR) source dipoles were introduced as intragranular dislocations in the grain region. The geometry of our atomic models was as follows: the average grain size d was $83a_0$ (a_0: lattice constant), and the length of the dislocation source L was 55 a_0, where a_0 = 3.615 Åfor Cu and a_0 = 4.05 Åfor Al. The dislocation density of the polycrystalline models was controlled by changing the number of FR sources (N_{FR}) within the grain region. Atomic models of cubic polycrystals containing 15 grains with and without FR sources in Cu and Al are presented in Fig. 1, where the dislocation density of $N_{\mathrm{FR}} = 6$ corresponds to 7.14×10^{15} and $5.67 \times 10^{15}\mathrm{m}^{-2}$ for Cu and Al, respectively, and the centrosymmetry parameter [35] was adjusted to visualize various defect structures. The polycrystalline model had dimensions of 220 a_0 on each side of the cube, including approximately 43 million atoms. (Dimensions of 330 a_0 with 102 million atoms were also used for a tensile test of $N_{\mathrm{FR}} = 0$ to verify the size effect.)

Parallelized molecular dynamics and visualization codes were developed using MPI-IO and applied to the collective defect dynamics of the large-scale atomic models, where MPI-IO was applied to ATOMEYE [36]. The embedded atom method (EAM) potential proposed by Mishin et al. was employed for the interatomic interaction of Cu and Al atoms [37, 38]. Uniaxial tension and compression were then applied to the atomic models, where a strain increment $\Delta\epsilon_{zz}$ of 1.0×10^{-3} was gradually applied. After applying tensile/compressive strain, the quasi-equilibrium configuration under the deformation at 0 K was obtained using molecular statics simulations combined with the conjugate gradient method. Triaxial periodic boundary conditions were satisfied during the uniaxial tensile/compressive loading, and the stress components perpendicular to the load direction were controlled to be zero during the relaxation steps. The atomic system under given strain was optimized by sufficient relaxation steps, and the fully relaxed configuration for each condition was defined as that when the maximum force of all atoms converged at 0.1 eV/Å, where the minimum number of relaxation is set to 4000 steps according to preliminary examinations [29]. This cycle was repeated until the maximum tensile/compressive strain reached 8%.

RESULTS AND DISCUSSION

The stress-stress curves for various initial dislocation densities corresponding to $N_{FR} = 0, 1, 4, 6$ under uniaxial tension and compression in Cu and Al are presented in Fig. 2; the yield stress, σ_Y was defined as the maximum stress in these curves. The yield stress decreased with increasing dislocation density under both tension and compression, and intragranular dislocations played a dominant role in the initial yield, as observed in coarse-grained metals. I have previously confirmed that the dependency of the initial dislocation density on yield stress is caused by heterogeneous stress distribution between grains [20]. There are only a few dislocation sources within a grain region, and dislocations are no longer homogeneously distributed as the initial dislocation density decreases. In addition, the flow stress relaxes to a certain value because the grain size and other grain geometrical parameters are identical in all of the models. In this study, I pay special attention to the difference in the asymmetric yield behavior between Cu and Al. The yield stress in Cu did not differ significantly depending on the loading orientation, whereas the initial dislocation density affected yield stress. However, the T/C asymmetry in Al was more significant with decreasing initial dislocation density as shown in Fig. 2(e); that is, the yield stress under tension was lower than that under compression. Here the degree of T/C asymmetry is expressed as $(\sigma_{\mathrm{Y}}^{\mathrm{C}} - \sigma_{\mathrm{Y}}^{\mathrm{T}})/(\sigma_{\mathrm{Y}}^{\mathrm{C}} + \sigma_{\mathrm{Y}}^{\mathrm{T}})$. The initial yield is ultimately caused by dislocation nucleation from the grain boundary when there is no intragranular dislocation. The difference in T/C asymmetry between UFG Al and UFG Cu is therefore expected to be attributed to the nucleation mechanism of dislocations from grain boundaries.

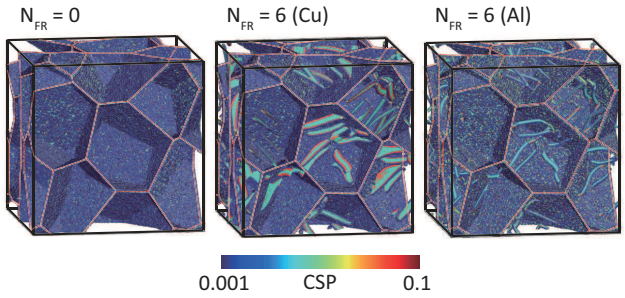

FIG. 1. (Color online) Atomic models of three-dimensional polycrystalline models (a) without intragranular defects and including intragranular dislocations in (b) Cu and (c) Al.

The stacking fault (SF) energy is a crucial property in determining plastic deformation behavior and describing nucleation process of dislocations from grain boundary in nanocrystalline metals [39, 40]. I focused on the high-stress condition achieved in UFG metals and investigated the effect of external stress on the SF energy and dislocation core properties. The generalized SF energy surfaces in terms of displacement along x and y directions for Cu and Al evaluated using the EAM potential are presented in Fig. 3(a) and (b), where the x, y, and z axes correspond to $\langle 1\bar{1}0\rangle$, $\langle 11\bar{2}\rangle$, and $\langle 111\rangle$, respectively. The energy difference along the $\mathbf{b}_{\mathrm{p}}$ direction determines the core structure of the dislocation, and the effect of tensile and compressive stresses on the SF energy is depicted in Fig. 3(b), where horizontal axis is the displacement normalized by the magnitude of Burgers vector of partial dislocation and γ_{SF} corresponds the stable stacking fault energy. Interestingly, γ_{SF} of Al was strongly affected by

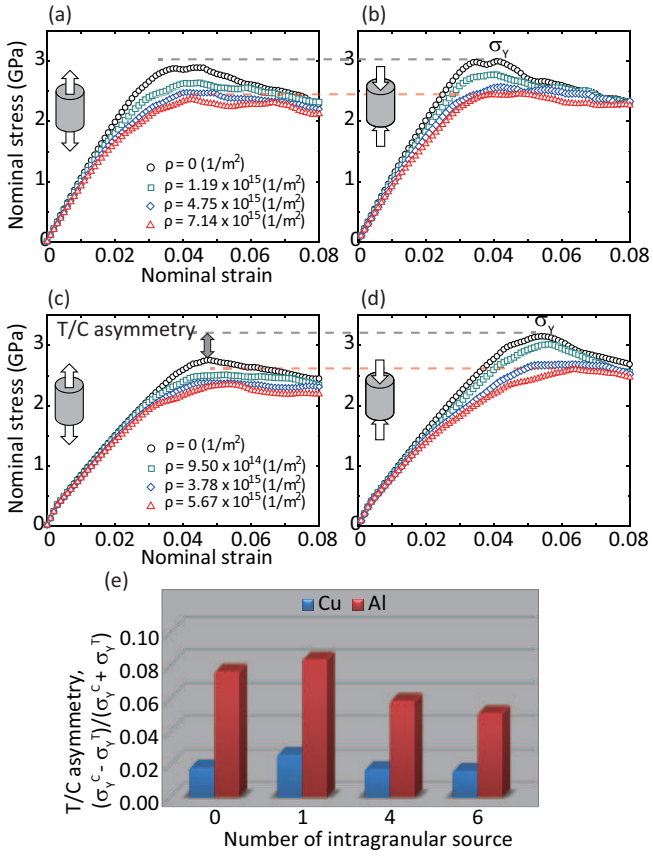

FIG. 2. (Color online) Stress-strain curves and T/C asymmetry in UFG metals with different dislocation densities under uniaxial stress: (a) Cu under tension, (b) Cu under compression, (c) Al under tension, and (d) Al under compression. (e) Difference in T/C asymmetry between Cu and Al and dependency of dislocation density.

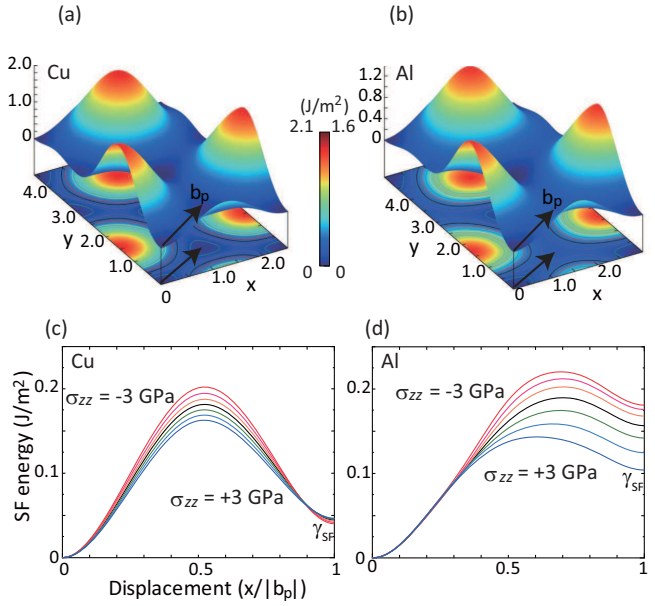

FIG. 3. (Color online) SF energy surfaces of (111) plane under zero stress in (a) Cu and (b) Al, where the direction of the minimum energy path corresponds to the $\langle 11\bar{2}\rangle$ direction. Effect of compressive and tensile stresses ($\sigma_{zz} = -3, -2, -1, 0, 1, 2, 3$ GPa) on the SF energy along $\langle 11\bar{2}\rangle$ direction in (c) Cu and (d) Al, where the SF energy under zero stress is represented by the black line and the compressive and tensile stresses are represented by the reddish and bluish lines, respectively.

the external stress, whereas that of Cu did not change greatly. These features have been addressed by the nature of the electronic structure and local atomic motion on the slip plane [41]. In contrast, the maximum residual stress, which is defined as the maximum gradient of energy difference along the $\langle 11\bar{2}\rangle$ direction ($\tau_{\max}$), was not affected by the external normal stress in Al. These finding indicates that the dislocation core structure of Al is strongly affected by the external stress rather than the Peierls stress according to the classical Peierls-Nabarro (PN) model [42, 43]. I examined a detailed dislocation core structure using the semidiscrete variational (SV) PN model [44, 45], which provides the three-dimensional dislocation core structure via discrete atomic rows and an accurate SF energy surface. I have previously confirmed that the SVPN model can successfully reproduce the dislocation core structure reflecting the change in SF energy [46]. In the SVPN framework, the total fault energy of a dislocation without applied shear stress and long-range interactions can be described as $U_{\text{disl}} = U_{\text{elastic}} + U_{\text{misfit}}$. The elastic energy contribution, U_{elastic}, was directly calculated using the energy factors of edge/screw dislocations associated with elastic constants, and the misfit energy contribution, $U_{misfit} = \sum_i \Delta x \gamma(\delta_i)$, was evaluated using the accurate SF energy surface, as shown in Fig. 3, where Δx is the distance between atomic row and $\gamma(\delta_i)$ is defined as the local misfit energy per area with lattice disregistry δ_i. As a result, the effect of the external stress on dislocation core was effectively considered by the stress-dependent SF energy. Dislocation core structures under compressive/tensile stresses in Cu and Al are depicted in Fig. 4, where horizontal axis is the nodal distance from the center of dislocation core and vertical axis shows the core density of a dislocation expressed by the local gradient of lattice disregistry ($\rho = (d\delta_x/dx)_{x=x_i} \simeq (\Delta\delta_i/\Delta x_i)$). A dislocation in Cu is known to be dissociated into two partial dislocations, and the core structure is not affected by either compressive or tensile stress. The dislocation core in Al is normally viewed as a nearly perfect dislocation, as demonstrated in Fig. 4(c) (under compression). However, the perfect dislocation tends to dissociate gradually with increasing tensile stress; that is, external tensile stress makes the extended dislocation more stable. This change in core structure is expected to affect dislocation nucleation at grain boundaries, which is considered to play a decisive role in the plastic deformation of UFG metals.

Pre-existing dislocations were initially activated in the early stage of deformation, where the critical resolved stress of intragranular dislocation differs little depending on the load direction. The activation of intragranular dislocations does not cause macroscopic yield because the plastic strain generated by a small amount of intragranular dislocation motion is

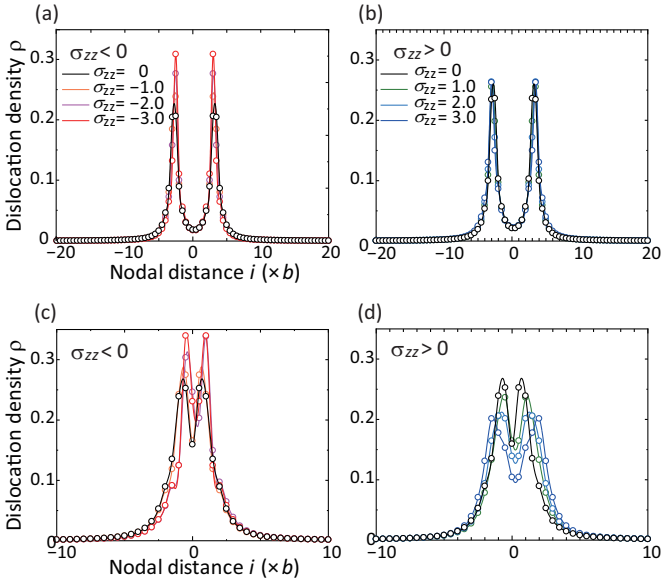

FIG. 4. (Color online) Dislocation core densities evaluated using SVPN model in Cu and Al, showing the effect of various external stress conditions on the core structure for (a) Cu under compression, (b) Cu under tension, (c) Al under compression, and (d) Al under tension.

small. In contrast, the nucleation process of dislocations from GBs, which corresponds to macroscopic yield of UFG metals differs completely depending on the external stress condition. The nucleation of dislocations from GBs under compression and tension for the $N_{\mathrm{FR}} = 1$ model for Al is shown in Fig. 5. Perfect-like dislocations were nucleated under compression, as observed in coarse-grained metals (Fig. 5(a)), whereas twinning deformation occurred under tension. In general, twinning deformation is more likely to be generated in low-SF-energy metals such as Cu and austenitic steel, whereas it is not observed in coarse-grained Al. As previously mentioned, a high stress condition is achieved in UFG metals, which significantly changes the SF energy of Al. In particular, high tensile stress causes a decrease of the SF energy, and dislocations tend to be dissociated into partial dislocations. The energy of a partial dislocation is one-third less than that of a perfect dislocation, which promotes the nucleation of partial dislocations from GBs. The emitted dislocation tends to extend and form multiple deformation twins because of the low SF energy under tension. Additionally, a dislocation is more likely to nucleate along a twin boundary (known as a displacement shift complete lattice dislocation) because the energy barrier of dislocation motion on a twin boundary is smaller than that of a perfect crystal [47]. Therefore, more dislocations are nucleated under tension than under compression. The T/C asymmetry of Al is caused by the dependence of the external stress on the core structure of the dislocation, which is associated with the SF energy. The rest of important features are temperature and strain rate dependency on deformation process. Recent accelerated molecular dynamics technique allows to capture the relationship between temperature/strain rate and dislocation nucleation from GBs [48]. According to the simple model simulation, it can be expected that the yield process in UFG metals is sensitive to the temperature due to a large activation entropy. Thus, the new mechanism of T/C asymmetry describes the unique nature of UFG metals and differs completely from the atomic-pair mechanism in NC and amorphous metals.

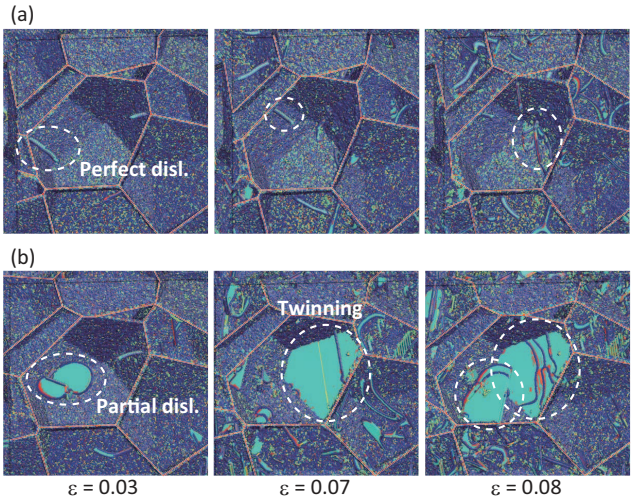

FIG. 5. (Color online) Evolution of defect structures for $N_{\mathrm{FR}} = 1$ model under (a) compression and (b) tension in UFG Al. The nucleation processes of perfect and partial dislocations from GBs are highlighted by the white dotted circles.

SUMMARY

In summary, I discussed the anomalous T/C asymmetry in UFG metals based on atomistic simulations and dislocation theory. Atomistic simulations revealed the remarkable T/C asymmetry of yield stress in UFG Al compared with that of UFG Cu. The yield event is not related to intragranular dislocation but caused by dislocation nucleation from GBs. I investigated the dependence of the nucleation process on the external stress from the viewpoint of the dislocation core structure. The SF energy of Al is strongly affected by the normal stress, and the application of tensile stress significantly decreases the SF energy. According to SVPN analysis combined with accurate SF energy calculations, the dislocation core is expected to dissociate into partial dislocations. Dislocations are therefore more likely to be nucleated from GBs because the energy of a partial dislocation is one-third less than that of a perfect one. Thus, the anomalous T/C asymmetry of UFG Al is explained by a new mechanism based on dependence of the stability of the dislocation core on the external stress, which is different from the well-known mechanisms of T/C asymmetry in hcp, NC, and amorphous metals and unique to high-strength UFG metals.

This work was supported by a Grant-in-Aid for Scientific Research (C) (No. 16K06714), Scientific Research on Innovative Areas (No. 22102007) and JST Collaborative Research Based on Industrial Demand "Heterogeneous Structure Control: Towards Innovative Development of Metallic Structural Materials."

[1] E. O. Hall, Proc. Phys. Soc. Lond. **64**, 747 (1951).
[2] N. J. Petch, J. Iron Steel Inst. **174**, 25 (1953).
[3] Y. Iwahashi, Z. Horita, M. Nemoto, J. Wang, and T. G. Langdon, Scripta Mater. **35**, 143 (1996).
[4] Y. Saito, H. Utsunomiya, N. Tsuji, and T. Sakai, Acta Mater. **47**, 579 (1999).
[5] R. Z. Valiev, Y. V. Ivanisenko, E. F. Rauch, and B. Baudelet, Acta Mater. **44**, 4705 (1996).
[6] S. H. Lee, Y. Saito, N. Tsuji, H. Utsunomiya, and T. Sakai, Scripta Mater. **46**, 281 (2002).
[7] X. Huang, N. Hansen, and N. Tsuji, Science **312**, 249 (2006).
[8] Y. M. Wang and E. Ma, Acta Mater. **52**, 1699 (2004).
[9] Y. Kimura, T. Inoue, F. Yin, and K. Tsuzaki, Science **320**, 1057 (2008).
[10] N. Tsuji, Y. Ito, Y. Saito, and Y. Minamino, Scripta Mater. **47**, 893 (2002).
[11] N. Kamikawa, X. Huang, N. Tsuji, and N. Hansen, Acta Mater. **57**, 4198 (2009).
[12] A. H. Chokshi, A. Rosen, J. Karch, and H. Gleiter, Scripta Metall. **23**, 1679 (1989).
[13] G. E. Fougere, J. R. Weertman, R. W. Siegel, and S. Kim, Scripta Metall. Mater. **26**, 1879 (1992).
[14] H. Conrad and J. Narayan, Appl. Phys. Lett. **81**, 2241 (2002).
[15] J. Schiøtz and K. W. Jacobsen, Science **301**, 1357 (2003).
[16] M. Y. Gutkin, I. A. Ovidfko, and N. V. Skiba, Acta Mater. **51**, 4059 (2003).
[17] T. Shimokawa, A. Nakatani, and H. Kitagawa, Phys. Rev. B **71**, 224110 (2005).
[18] M. Haouaoui, I. Karaman, and H. J. Maier, Acta Mater. **54**, 5477 (2006).
[19] J. Rajagopalan, R. Christian, H. P. Karntharler, D. Gerhard, and M. T. A. Saif, Acta Mater. **58**, 4772 (2010).
[20] T. Tsuru, Y. Aoyagi, Y. Kaji, and T. Shimokawa, Model. Simul. Mater. Sci. Eng. **24**, 035010 (2016).
[21] J. E. Carsley, A. Fisher, W. W. Milligan, and E. C. Aifantis, Metall. Mater. Trans. A **29**, 2261 (1998).
[22] R. W. Hayes, R. Rodriguez, and E. J. Lavernia, Acta Mater. **49**, 4055 (2001).
[23] S. Cheng, J. A. Spencer, and W. W. Milligan, Acta Mater. **51**, 4505 (2003).
[24] A. Singh, H. Somekawa, and T. Mukai, Scripta Mater. **56**, 935 (2007).
[25] K. Máthis, J. Čapek, Z. Zdražilová, and Z. Trojanová, Mater. Sci. Eng. A **528**, 5904 (2011).
[26] A. Vinogradov, D. Orlov, A. Danyuk, and Y. Estrin, Mater. Sci. Eng. A **621**, 243 (2015).
[27] L. Y. Chen, B. Z. Li, X. D. Wang, F. Jiang, Y. Ren, P. K. Liaw, and J. Z. Jiang, Acta Mater. **61**, 1843 (2013).
[28] J. R. Trelewics and C. A. Schuh, Acta Mater. **55**, 5948 (2007).
[29] "See supplemental material at http:// for the technical details and preliminary comparison with nanocrystalline metals,".
[30] J. Schiøtz, T. Vegge, F. D. DiTolla, and K. W. Jacobsen, Phys. Rev. B **60**, 11971 (1999).
[31] H. Van Swygenhoven, P. M. Derlet, and A. Hasnaoui, Phys. Rev. B **66**, 024101 (2002).
[32] H. Van Swygenhoven and P. M. Derlet, Phys. Rev. B **64**, 224105 (2001).
[33] A. C. Lund, T. G. Nieh, and C. A. Schuh, Phys. Rev. B **69**, 012101 (2004).
[34] A. M. Dongare, A. M. Rajendran, B. LaMattina, M. A. Zikry, and D. W. Brenner, Comput. Mater. Sci. **49**, 260 (2010).
[35] C. L. Kelchner, S. J. Plimpton, and J. C. Hamilton, Phys. Rev. B **58**, 11085 (1998).
[36] J. Li, Model. Simul. Mater. Sci. Eng. **11**, 173 (2003).
[37] Y. Mishin, M. J. Mehl, D. A. Papaconstantopoulos, A. F. Voter, and J. D. Kress, Phys. Rev. B **63**, 224106 (2001).
[38] Y. Mishin, D. Farkas, M. J. Mehl, and D. A. Papaconstantopoulos, Phys. Rev. B **59**, 3393 (1999).
[39] V. Yamakov, D. Wolf, S. R. Phillpot, A. K. Mukherjee, and H. Gleiter, Nature Mater. **3**, 43 (2004).
[40] H. Van Swygenhoven, P. M. Derlet, and A. G. Froseth, Nature Mater. **3**, 399 (2004).
[41] S. Ogata, J. Li, and S. Yip, Science **2002**, 807 (298).
[42] R. Peierls, Proc. Phys. Soc. **52**, 34 (1940).
[43] F. R. N. Nabarro, Proc. Phys. Soc. **59**, 256 (1947).
[44] V. V. Bulatov and E. Kaxiras, Phys. Rev. Lett. **78**, 4221 (1997).
[45] G. Lu, N. Kioussis, V. V. Bulatov, and E. Kaxiras, Phys. Rev. B **62**, 3099 (2000).
[46] T. Tsuru, Y. Udagawa, M. Yamaguchi, M. Itakura, H. Kaburaki, and Y. Kaji, J. Phys.: Condens. Matter. **25**, 022202 (2013).
[47] T. Tsuru, Y. Kaji, D. Matsunaka, and Y. Shibutani, Phys. Rev. B **82**, 024101 (2010).
[48] J.-P. Du, Y.-J. Wang, Y.-C. Lo, L. Wan, and S. Ogata, Phys. Rev. B **94**, 104110 (2016).